

Mössbauer Studies of Fe⁵⁷ in Orthoferrites*

M. EIBSCHÜTZ, S. SHTRIKMAN, AND D. TREVES†

Department of Electronics, The Weizmann Institute of Science, Rehovoth, Israel

(Received 31 October 1966)

The hyperfine interactions of the iron nuclei in the orthoferrites were studied between 85 and 770°K using the Mössbauer effect. The temperature dependence of the sublattice magnetization $\sigma_s(T)$ is compared with various statistical-mechanical theories. It obeys approximately a $\frac{1}{3}$ power law in the temperature range $0.60 < T/T_N < 0.99$, and spin-wave theory and Callen decoupling at low temperature in the range $T/T_N < 0.5$. From $\sigma_s(T)$, it is found that the canting angle in these weak ferromagnets is temperature-independent. The exchange integral calculated from the Oguchi spin-wave theory agrees with that calculated from Rushbrook and Wood's high-temperature series expansion and the Green's-function theories, while that calculated from the molecular field and Kubo's spin-wave theories is considerably lower. The quadrupole coupling constant is in good agreement with values calculated by point-charge lattice sums. The specific heat obtained from the temperature shift at high temperature agrees with the Dulong-Petit law. The value of the isomer shift is equal to that expected for a trivalent iron ion.

1. INTRODUCTION

FOR some time, our laboratory has been engaged in a comprehensive study of the magnetic properties of the orthoferrites. This program covered the crystallography of these materials^{1,2} and its relation to their magnetic properties,³ the magnetic structure,⁴ the behavior of the ferromagnetic moment,⁵ susceptibility, and field-dependent susceptibility.^{4,6} As part of this program, Mössbauer studies in these materials were also carried out, and these studies are the subject of the present paper. Reference to the work of other groups on the orthoferrites can be found in Ref. 7.

The orthoferrites have the formula $R\text{FeO}_3$, with R a rare earth. Their space group is^{8,9} $Pbnm$, which is a distorted perovskite. The crystallographic unit cell, shown in Fig. 1, contains four equivalent iron ions. The distortion of the perovskite structure is such that the iron environment remains essentially octahedral; however, the axes of the four octahedral sites are in different directions. The environment of the R ions is, however, far from cubic.² The iron ions form a distorted simple cubic lattice and alternate with oxygen ions along the $\langle 100 \rangle$ directions of this simple cubic structure. One can visualize the structure as a three-dimensional network of strings of oxygen octahedra, whose axes zigzag slightly. At the center of each octahedron, there is an

iron ion. The common apex of two adjacent octahedra is the intervening anion that provides the superexchange bond between two iron ions. Thus, each iron ion is coupled by superexchange to six iron nearest neighbors, resulting in high Néel temperatures. The degree of zigzagging of the octahedra is determined to a large extent by the size of the R ions that are located in the interstices between the octahedra. The larger the R , the more the chains of octahedra stretch, the zigzagging decreases, and the superexchange bond angle approaches 180 deg³. Thus, LaFeO_3 has the highest Néel point and LuFeO_3 the lowest. The Néel point of YFeO_3 falls between that of DyFeO_3 and that of HoFeO_3 , as expected from the size of the Y^{3+} ion.¹⁰

The magnetic ordering of the iron ions is essentially antiferromagnetic (see Fig. 1). However, the symmetry of the magnetic unit cell, which is equal to the crystallographic one,¹¹ is low, so that weak ferromagnetism is allowed¹² and is actually found. (See Ref. 4 and references therein.) The crystallographic symmetry allows only two independent superexchange constants for the 6 nearest-neighbor bonds of each iron ion: 4 of one kind, through the O_{II}^{2-} ions, and 2 of the other through the O_I^{2-} ions^{2,3,8,9} (see Fig. 1). These are expected to be similar in value, and because of the perovskite structure, any other Fe-Fe coupling is very much smaller.¹³ Magnetic couplings of the type Fe- R ⁵ and R - R ¹⁴ are at least two orders of magnitude below the Fe-Fe coupling. This relatively simple magnetic situation, the intriguing weak ferromagnetic properties, the large number of materials belonging to this family, and their availability made us choose the orthoferrites as the subject of this work.

* Work supported in part by Air Force Materials Laboratory, Research and Technology Division AFSC, through the European Office of Aerospace Research, U. S. Air Force.

† Temporary address: Ampex Corporation, Redwood City, California.

¹ M. Eibschütz, *Acta Cryst.* **19**, 337 (1965).

² P. Coppens and M. Eibschütz, *Acta Cryst.* **19**, 524 (1965).

³ D. Treves, M. Eibschütz, and P. Coppens, *Phys. Letters* **18**, 216 (1965).

⁴ D. Treves, *Phys. Rev.* **125**, 1843 (1962); G. Gorodetsky and D. Treves, *ibid.* **135**, A797 (1964).

⁵ G. Gorodetsky and D. Treves, in *Proceedings of the International Conference on Magnetism, Nottingham, 1964* (The Institute of Physics and The Physical Society, London, 1965), p. 606.

⁶ Yc. A. Turov and V. Ye Haysh, *Phys. Metals Metallog.* (USSR) **9**, 7 (1960).

⁷ D. Treves, *J. Appl. Phys.* **36**, 1033 (1965).

⁸ S. Geller and E. A. Wood, *Acta Cryst.* **9**, 536 (1956).

⁹ S. Geller, *J. Chem. Phys.* **24**, 1236 (1956).

¹⁰ M. Eibschütz, G. Gorodetsky, S. Shtrikman, and D. Treves, *J. Appl. Phys.* **35**, 1071 (1964).

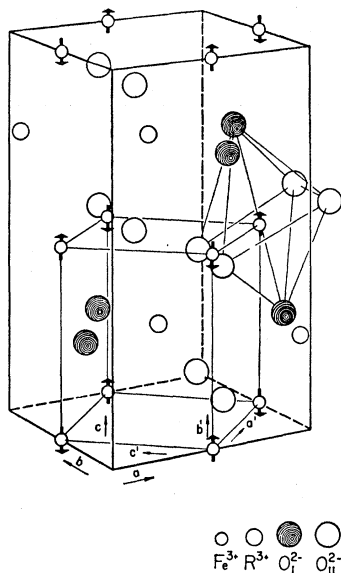
¹¹ W. C. Koehler and E. O. Wolan, *J. Phys. Chem. Solids* **2**, 100 (1957); W. C. Koehler, E. O. Wolan, and M. K. Wilkinson, *Phys. Rev.* **118**, 58 (1960).

¹² I. E. Dzyaloshinsky, *J. Phys. Chem. Solids* **4**, 241 (1958).

¹³ G. Blasse, *Philips Res. Rept.* **20**, 327 (1965).

¹⁴ R. M. Bozorth, H. J. Williams, and D. E. Walsh, *Phys. Rev.* **103**, 572 (1956).

FIG. 1. The unit cell of the orthoferrites $R\text{FeO}_3$. The monoclinic pseudocell is indicated by a' , b' , c' . The vectors indicate the magnetic ordering of iron ions. Notice the tilting of the octahedra around the Fe^{3+} .



The main purpose of the Mössbauer work, of which some preliminary results have already been published in the literature,^{10,15} was to measure the temperature dependence of the sublattice magnetization. This was needed in order to obtain additional evidence with respect to the origin of weak ferromagnetism in the orthoferrites,^{16,4} and to gain insight into the nature of the R - Fe coupling.⁵ These measurements were also compared with various theories of the temperature dependence of the sublattice magnetization.

The same measurements could have been done, at least in principle, with nuclear magnetic resonance or neutron diffraction. Preliminary attempts failed to find the nuclear resonance of these materials, and the precision of the neutron-diffraction method is inadequate for our purpose, particularly near the Néel point.¹¹ We therefore used the present Mössbauer studies.

II. EXPERIMENTAL PROCEDURE AND RESULTS

The Mössbauer spectra were obtained in part on a spectrometer of our design¹⁷ and in part on a commercial one.¹⁸ The spectra were automatically plotted on an x - y recorder, and the data were read from the graphs using a ruler. The energy-splittings spectra of $\alpha\text{Fe}_2\text{O}_3$ were routinely taken for calibration of the Mössbauer spectrometer (515 kOe at room temperature). A 2-mCi Co^{57} source on chromium (Nuclear Science and Engineering Corporation, Pittsburgh, Pennsylvania) and a 5-mCi Co^{57} copper (New England Nuclear Corporation, Boston, Massachusetts) were used. Both gave, with a

thin $\text{K}_4\text{Fe}(\text{CN})_6 \cdot 10\text{H}_2\text{O}$ absorber, a linewidth of 0.25 mm/sec. In all the measurements, the source was at room temperature, and was driven by the velocity transducer.¹⁷ The materials to be studied, which were the absorbers, were stationary and in a cryofurnace¹⁹ that allowed control and stabilization of the temperature within 1°K for many hours in the range 85–770°K.

The orthoferrite absorbers were prepared by ceramic methods from the oxides $R_2\text{O}_3$ and Fe_2O_3 . The latter was enriched between 30 and 90% with Fe^{57} . The purity of the oxides was greater than 99.9%. The oxides were pre-fired for two hours at 900°C and then reground and fired for 16 h at 1400°C in air. Unenriched samples were simultaneously prepared, and x-ray checked to ensure that the products were single-phase materials.

All the orthoferrites yielded simple 6-line spectra below the Néel temperature T_N , and an unsplit line above T_N in agreement with the existence of only one type of crystallographic site of the iron ion. Typical unretouched spectra of DyFeO_3 between room temperature and T_N , and of PrFeO_3 near T_N , are shown in Figs. 2 and 3, respectively. The absorbers were quite thick (the Mössbauer effect of the outermost absorption peaks below T_N was of the order of 25%), so that the ratio of the intensities of the lines below T_N departed from the ratio 1:2:3.

From Fig. 3, one can observe that, near T_N , defined by the temperature at which the splitting disappears, the temperature resolution is of the order of 1°K. Thus the Mössbauer effect is a good means for determining T_N , which was found in good agreement with other techniques.^{7,10} The values of T_N measured by the Mössbauer effect are given in Table I. The difference between these values and those given in Ref. 7 is due to an improved temperature-measuring technique.

In Fig. 3, there appears to be a range in temperature near T_N in which a paramagnetic peak coexists with the split spectrum typical of ordered magnetic materials. This coexistence is presumably associated with the critical fluctuations of the magnetization near the transition point.²⁰ A similar behavior was found in the Mössbauer spectra of some superparamagnetic powders.²¹

TABLE I. The canting angle α and the Néel temperature T_N in orthoferrites.

R	α (mrad)	T_N (°K)	R	α (mrad)	T_N (°K)
La	9.1	740	Dy	8.0	645
Pr	8.5	707	Y	8.9	640
Nd	8.5	687	Ho	8.2	639
Sm	8.2	674	Er	8.1	636
Eu	8.0	662	Tm	8.0	632
Gd	9.8	657	Yb	8.9	627
Tb	7.8	647	Lu	10.7	623

¹⁵ J. Chappert and P. Inbert, J. Phys. Radium **24**, 412 (1963).

¹⁶ T. Moriya, Phys. Rev. **120**, 91 (1960).

¹⁷ J. Lipkin, B. Schechter, S. Shtrikman, and D. Treves, Rev. Sci. Instr. **35**, 1336 (1964).

¹⁸ Elron Electronics Industries, Ltd., Haifa, Israel.

¹⁹ B. Sharon and D. Treves, Rev. Sci. Instr. **37**, 1252 (1966).

²⁰ L. Pal (private communication).

²¹ W. I. Shuele, S. Shtrikman, and D. Treves, J. Appl. Phys. **36**, 1010 (1965).

TABLE II. Numerical results of Mössbauer-effect measurements in orthoferrites.

T^a (°K)	H_n^b (kOe)	ΔE^c (mm/sec)	ϵ^d (mm/sec)	T^a (°K)	H_n^b (kOe)	ΔE^c (mm/sec)	ϵ^d (mm/sec)
LaFeO ₃							
0	564						
85	562	0.61	-0.020	562	391	0.34	-0.017
167	554	0.60	-0.025	604	359	0.30	-0.025
223	541	0.56	-0.026	661	299	0.26	-0.025
240	539	0.55	-0.020	701.5	233	0.23	-0.037
249	535	0.54	-0.036	710.5	214	0.23	-0.025
296	521	0.54	-0.020	721	180	0.23	-0.020
402	483	0.46	-0.027	731	140	0.21	-0.025
480	445	0.40	-0.022	734	116	0.21	-0.033
526	419	0.36	-0.016				
PrFeO ₃							
0	559						
85	557	0.60	-0.006	515	405	0.34	-0.009
150	553	0.58	-0.007	571	364	0.32	0.000
208	538	0.57	-0.002	632	295	0.26	-0.024
254	529	0.53	-0.010	673	219	0.26	-0.002
296	510	0.50	-0.012	692	158	0.22	-0.005
384	479	0.46	-0.024	698.5	141	0.22	-0.016
464	439	0.40	-0.005				
NdFeO ₃							
0	557						
85	554	0.60	-0.024	609	302	0.30	-0.008
297	508	0.52	-0.005	631	270	0.27	-0.022
376	476	0.46	0.002	645	243	0.28	-0.008
436	443	0.43	0.028	658	215	0.27	-0.005
484	417	0.39	-0.011	668	181	0.26	-0.027
535	377	0.35	-0.002	671	172	0.26	-0.019
577	340	0.33	-0.005	676	149	0.26	-0.008
				681	118	0.24	-0.020
SmFeO ₃							
	552						
85	550	0.63	-0.045	492	406	0.41	-0.011
142	542	0.62	-0.047	508	392	0.40	-0.005
219	526	0.57	-0.051	537	367	0.37	-0.014
296	503	0.54	-0.054	579	328	0.35	0.014
309	500	0.54	-0.061	611	282	0.33	0.023
335	493	0.54	-0.052	636	236	0.30	0.026
377	472	0.50	-0.029	658	167	0.26	0.006
445	436	0.46	-0.015	665	138	0.24	0.008
476	411	0.42	-0.017				
EuFeO ₃							
0	552						
85	550	0.63	0.018	594	295	0.32	0.017
296	510	0.50	0.024	602	283	0.32	0.012
335	494	0.50	0.011	608	273	0.32	0.011
369	480	0.49	0.005	615	259	0.29	0.005
411	459	0.46	0.012	622	245	0.29	0.005
463	427	0.41	0.014	627	230	0.29	0.006
505	397	0.39	0.025	636	206	0.30	0.008
536	368	0.35	0.005	646	175	0.29	0.015
565	335	0.33	0.005	652	145	0.29	0.026
587	306	0.34	0.014	656	101	0.29	0.015
GdFeO ₃							
0	551						
85	549	0.61	0.010	583	296	0.31	0.011
296	502	0.57	0.029	611	254	0.31	0.014
323	491	0.52	0.023	626	216	0.31	0.026
367	469	0.51	0.026	633	197	0.30	0.029
399	455	0.47	0.024	640	175	0.28	0.011
443	435	0.45	0.008	646	144	0.26	0.023
473	409	0.41	0.000	651	116	0.25	0.038
509	382	0.40	0.017	653	104	0.25	0.014
538	356	0.38	0.032	655	92	0.25	0.039
560	335	0.37	0.029				
TbFeO ₃							
0	550						
85	548	0.62	0.018	580	276	0.32	0.021
296	500	0.53	0.018	612	226	0.29	0.020
364	469	0.49	0.029	620	207	0.30	0.033
419	439	0.46	0.018	627	185	0.28	0.002
466	407	0.39	0.003	637	155	0.29	0.002
530	353	0.35	0.014	642	127	0.28	-0.002
563	313	0.33	0.032	644	103	0.28	0.002

^a T = temperature; standard error $\pm 1^\circ\text{K}$.

^b H_n = internal field; standard error $\pm 2\text{kOe}$. The internal field at zero $^\circ\text{K}$ is calculated from Oguchi's spin-wave theory.

^c ΔE = shift; standard error $\pm 0.01\text{ mm/sec}$.

^d ϵ = quadrupole coupling; standard error $\pm 0.03\text{ mm/sec}$.

TABLE II. (continued).

T^a (°K)	H_n^b (kOe)	ΔE^c (mm/sec)	ϵ^d (mm/sec)	T^a (°K)	H_n^b (kOe)	ΔE^c (mm/sec)	ϵ^d (mm/sec)
DyFeO ₃							
0	548			582	289	0.34	0.000
85	546	0.62		601	257	0.30	0.008
296	498	0.54	0.025	615	225	0.27	0.000
343	477	0.51	0.014	626	191	0.28	-0.009
385	457	0.46	0.014	630	173	0.27	0.006
428	433	0.44	0.008	635	148	0.28	0.007
476	397	0.44	0.048	638.5	117	0.27	
527	357	0.38	0.026	642	75.6	0.26	
567	314	0.34	0.037				
YFeO ₃							
0	549			527	348	0.36	0.020
85	547	0.60	-0.002	561	308	0.34	-0.002
164	547	0.59	-0.008	586	270	0.34	0.002
296	495	0.52	0.010	604	232	0.31	-0.008
340	477	0.51	0.005	617	193	0.30	0.021
379	457	0.51	0.014	623	167	0.29	0.002
418	435	0.46	0.014	631	115	0.30	0.011
459	409	0.43	-0.008	633	104	0.30	0.000
500	376	0.38	0.014				
HoFeO ₃							
0	548			564	306	0.33	0.015
85	546	0.62	0.004	587	273	0.31	0.015
296	496	0.52	0.013	606	235	0.29	0.005
334	478	0.52	0.008	612	212	0.28	0.009
369	462	0.47	0.002	617	200	0.28	0.025
401	445	0.44	0.024	625	170	0.27	0.006
425	423	0.44	0.024	629	145	0.28	0.011
455	412	0.41	0.008	632	115	0.27	0.029
493	382	0.39	-0.011	634	91		
525	353	0.38	0.012				
553	325	0.34	0.012				
ErFeO ₃							
0	546			525	344	0.38	-0.002
85	544	0.63	-0.019	548	322	0.37	0.006
215	523	0.57	-0.014	562	303	0.31	-0.011
296	494	0.52	0.002	592	249	0.30	0.012
332	479	0.51	0.010	605	220	0.30	0.008
378	455	0.49	0.000	615	194	0.30	-0.002
404	440	0.44	0.006	622	164	0.29	0.000
446	414	0.41	-0.014	627	130	0.28	0.012
476	393	0.41	0.014	630	108	0.25	0.014
504	367	0.37	-0.023				
TmFeO ₃							
0	545			555	307	0.33	0.005
85	543	0.62	-0.021	569	291	0.34	0.011
215	521	0.56	-0.004	583	259	0.32	0.011
296	492	0.52	0.002	593	245	0.30	0.002
326	479	0.51	0.004	601	224	0.29	-0.018
380	453	0.43	-0.015	608	206	0.29	-0.017
416	433	0.44	0.027	612	189	0.30	-0.015
447	414	0.40	-0.005	618	166	0.29	-0.011
481	384	0.39	-0.005	623	138	0.30	-0.008
509	360	0.38	-0.002	626	120	0.25	-0.047
538	330	0.36	0.008				
YbFeO ₃							
0	546.5			534	345	0.42	-0.014
85	544	0.56	-0.020	551	310	0.36	0.008
296	491	0.51	-0.010	570	281	0.32	-0.014
317	481	0.48	0.006	597	223	0.30	0.000
349	468	0.48	-0.005	612	178	0.28	-0.011
373	453	0.47	-0.012	617	148	0.28	0.020
417	431	0.43	-0.005	622	112	0.27	-0.025
450	406	0.42	-0.021				
482	383	0.41	0.002				
LuFeO ₃							
0	545.5			560	296	0.33	-0.008
85	543	0.63	-0.015	579	262	0.33	0.000
213	519	0.58	-0.028	589	242	0.29	-0.040
296	490	0.51	0.018	598	215	0.31	-0.027
358	466	0.48	-0.020	601	204	0.28	-0.053
405	440	0.44	-0.027	609	182	0.26	-0.014
447	410	0.44	-0.019	615	145	0.26	-0.024
481	383	0.36	-0.014	621	84	0.25	
511	354	0.37	-0.024				
559	297	0.35	-0.018				

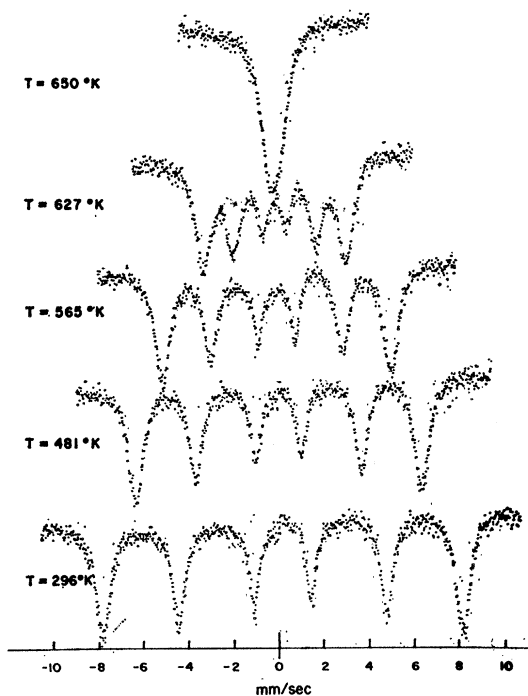


FIG. 2. Typical Mössbauer spectra for DyFeO_3 between room temperature and the Néel temperature. The source ^{57}Co in Cu was at room temperature; counting time was 10 sec with 80 000 counts/channel and about 60 channels/mm/sec.

The spectra were analyzed conventionally to give the internal field H_n , the quadrupole coupling ϵ , and the shift ΔE with respect to a Co^{57} in Cr source. The results are summarized in Table II. (Since the quad-

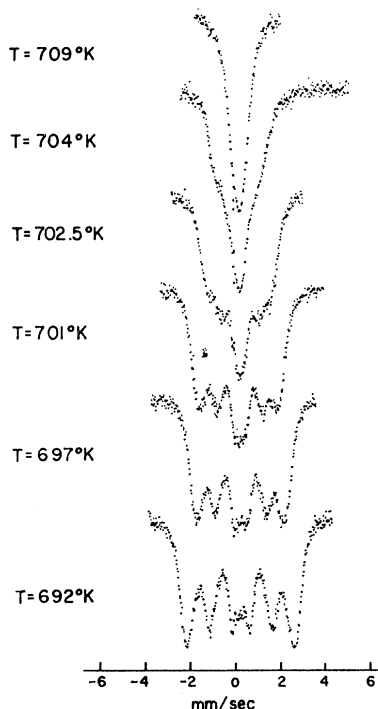


FIG. 3. Mössbauer spectra in the region of the Néel temperature for PrFeO_3 . The single line source (Co^{57} in Cr) was at room temperature. The counting time was 10 sec with 16 000 counts/channel.

rupole coupling is small compared to the magnetic splitting, we only measured the contribution of the electric field gradient along the direction of the sublattice magnetization.)

Graphs showing the temperature dependence of H_n are given in Fig. 4 for LaFeO_3 and LuFeO_3 . The results for the other orthoferrites fall between these two curves (with the exception of EuFeO_3 , which deviates above the curves less than the difference between the two curves). The quadrupole coupling $\frac{1}{4}eQV_{zz}$, where x is the direction of the sublattice magnetization, as a function of the atomic number R and of temperature is plotted in Figs. 14 and 15 respectively, and the isomer shift in Figs. 16 and 17.

The ratio of the nuclear magnetic moment of the excited state of Fe^{57} to that of the ground state, μ_1/μ_0 ,

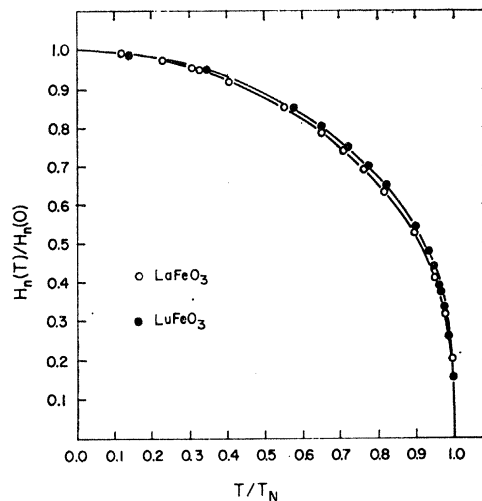


FIG. 4. Internal magnetic field $H_n(T)$ normalized to the value $H_n(0)$ at absolute zero as a function of the reduced temperature $t = T/T_N$ for LaFeO_3 and LuFeO_3 .

was calculated for about 100 room-temperature spectra. The average value was -1.712 ± 0.013 . Taking $\mu_0 = 0.0903 \pm 0.0007$ nm,²² one gets $\mu_1 = -0.1545 \pm 0.0024$, in good agreement with the literature.²³

III. DISCUSSION OF THE EXPERIMENTAL RESULTS

We assume that the internal field at the iron nucleus Fe^{3+} as a function of temperature is proportional to the sublattice magnetization.²⁴⁻²⁶

²² G. W. Ludwig and H. H. Woodbury, Phys. Rev. **117**, 1286 (1960).

²³ R. S. Preston, S. S. Hanna, and J. Heberle, Phys. Rev. **128**, 2207 (1962).

²⁴ V. Jaccarino, *Magnetism* (Academic Press Inc., New York, 1965), Vol. II A, p. 307.

²⁵ J. J. Van Loef and I. J. M. Froussien, Phys. Letters **7**, 225 (1963).

²⁶ S. Hufner, P. Kienle, W. Wiederman, J. Frey, and W. Zinn, in *Proceedings of the International Conference on Magnetism, Nottingham, 1964* (The Institute of Physics and The Physical Society, London, 1965).

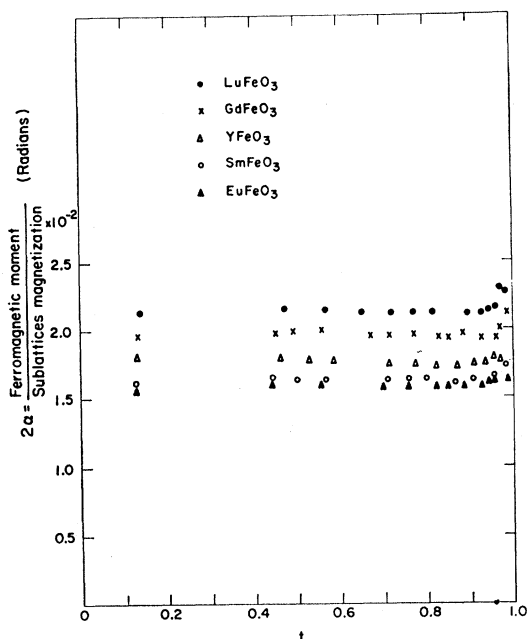


FIG. 5. Canting angle α versus reduced temperature $t = T/T_N$.

The relatively large range in temperature covered by this work and its accuracy make it possible to compare the experimental results with several statistical mechanical theories of magnetization, and perhaps to get some indication about their validity.

A. The Origin of the Weak Ferromagnetism

The iron ions in the orthoferrites are arranged essentially as two sublattices strongly coupled antiferromagnetically and slightly canted with respect to the antiferromagnetic axis, so that a small net ferromagnetic moment σ results in a direction perpendicular to the antiferromagnetic axis. The angle between the sublattice magnetization and the antiferromagnetic axis at zero external field is the canting angle α . This angle is determined by the ratio of perturbing forces, either of crystal-field or exchange origin,¹⁶ to the superexchange force. The dependence of α on temperature sheds light on the perturbing mechanism.

In orthoferrites with diamagnetic R ions, La^{3+} , Y^{3+} , Lu^{3+} , the measured ferromagnetic moment M is totally due to canting, so that $M = \sigma$. The angle α is given by

$$\alpha = \frac{1}{2} M / \sigma_s, \quad (1)$$

where σ_s is the iron sublattice moment. M was measured by conventional methods,⁵ while σ_s was obtained from the Mössbauer work. In Fig. 5 are given the values of α as a function of temperature for YFeO_3 and LuFeO_3 , assuming that $\sigma_s(0) = 5$ Bohr magneton.

In the case of paramagnetic R ions, the situation is slightly more involved, as these are coupled to some extent to the iron ions, so that they also contribute to

the total ferromagnetic moment M . The fact that the R -Fe coupling⁵ is only of the order of degrees K leads one to assume that at reasonably high temperature the R ions will behave as a paramagnet in an effective field proportional to the iron sublattice moment⁵ σ_s . Thus

$$M = 2\alpha\sigma_s(1 + dt^{-1}), \quad (2)$$

where $t = T/T_N$ and d is an interaction parameter.

A plot of Mt/B as a function of temperature, where M is the experimentally measured ferromagnetic moment and $B = \sigma_s(t)/\sigma_s(0)$, as taken from the Mössbauer data should, according to (2), follow the line $2\alpha\sigma_s(0) \times (t+d)$. Typical examples are shown in Fig. 6. The intercept with $t=0$ yields d and, assuming $\sigma_s(0) = 5$ Bohr magnetons, one finds $\alpha(t)$, which is plotted for a few orthoferrites in Fig. 5. From this figure, one can see that α is essentially temperature-independent; its value for all the orthoferrites is given in Table I.

The fact that α is constant over a very large temperature range indicates that the superexchange and perturbing force have the same temperature dependence, thus indicating that antisymmetric exchange¹⁶ is responsible for the canting and the weak ferromagnetism. This same conclusion was arrived at from other independent experiments.^{6,7}

B. The Superexchange Linkage Angle $\text{Fe}^{3+}\text{-O}^{2-}\text{-Fe}^{3+}$

Before proceeding with the comparison of various theories with the experimental results, a few general remarks about the exchange constant $|J|$ are appropriate. This parameter appears in most theories as proportional to the Néel temperature. Experimentally, a correlation is found between T_N and the superex-

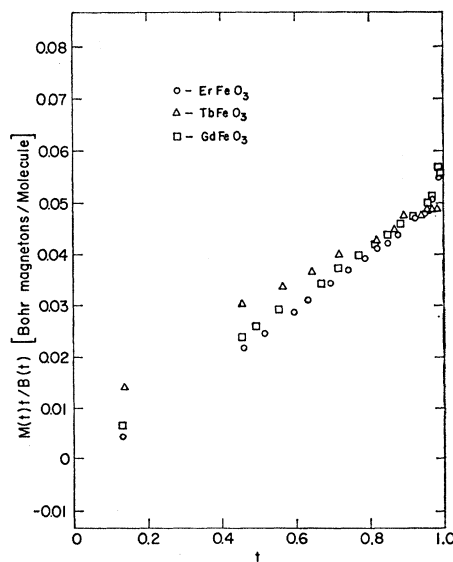


FIG. 6. Typical curves $Mt\sigma_s(0)/\sigma_s(t)$ versus reduced temperature $t = T/T_N$, where M is the total ferromagnetic moment and σ_s is the sublattice magnetization.

TABLE III. The exchange integral $|J|k^{-1}[^{\circ}\text{K}]$ in orthoferrites.

	La	Pr	Nd	Sm	Eu	Gd	Tb	Dy	Y	Ho	Er	Tm	Yb	Lu	error
Molecular field T_N	41	40.4	39.3	38.5	37.8	37.5	37.0	36.9	36.5	36.5	36.3	36.1	35.8	35.6	± 0.1
Kubo's (Ref. 30) spin waves	39	38	38	38	39	37	37	37	36	36	35	35	35	36	± 2
High-temperature expansion									56					48	
Perpendicular susceptibility [molecular field (Ref. 27)]									53					48.5	
Perpendicular susceptibility [Oguchi's spin-wave theory (Ref. 31)]									50.5					46.5	
Rushbrooke and Wood's T_N (Ref. 29)	59.0	56.3	54.7	53.7	52.7	52.3	51.5	51.4	50.9	50.9	50.7	50.4	50.0	49.6	± 0.1
Oguchi's spin-wave theory (Ref. 31)	58	56	54	53	53	52	52	52	51	51	51	51	50	50	± 5
RPA (Ref. 32)	64.2	61.4	59.6	58.5	57.5	57.0	56.2	56.0	55.5	55.5	55.2	54.9	54.4	54.1	± 0.1
CD (Ref. 32)	55.3	52.8	51.3	50.4	49.5	49.1	48.4	48.2	47.8	47.8	47.5	47.2	46.9	46.6	± 0.1

change bond angle Φ such that T_N , and thus $|J|$, is approximately given by³

$$T_N = T_N(0) \cos\Phi. \quad (3)$$

The accuracy of this relation is shown in Fig. 7, in which the calculated values, following (3), normalized for YFeO_3 , and the measured values of T_N as a function of the atomic number of R are given. The angle Φ was deduced from x-ray studies.¹⁻³

C. The Molecular-Field Theory

This theory covers the whole range of temperatures. One of its main theoretical relations that applies to the orthoferrites is

$$|J| = 3kT_N/ZS(S+1). \quad (4)$$

Here, k is Boltzmann's constant, $Z=6$ is the number of nearest neighbors, and $S=\frac{5}{2}$ for Fe^{3+} . $|J|$ is defined by the Hamiltonian

$$\mathcal{H} = +|J| \sum_{\langle i,j \rangle} \mathbf{S}_i \cdot \mathbf{S}_j, \quad (5)$$

where each nearest-neighbor pair $\langle i,j \rangle$ appears only

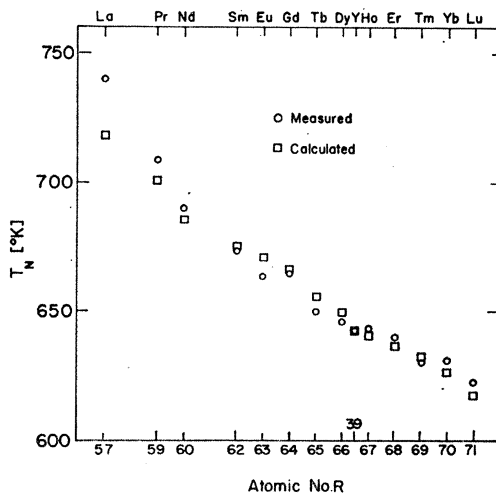


FIG. 7. Experimental and calculated Néel temperature as a function of the atomic rare-earth number R .

once in the summation. Also found from the molecular-field theory is the relation

$$\sigma_s(T)/\sigma(0) = B_{5/2} \left(\frac{3S}{S+1} \frac{\sigma_s(T)/\sigma_s(0)}{t} \right), \quad (6)$$

whose solution yields the temperature dependence of the sublattice magnetization. $B_{5/2}$ is the Brillouin function for the case $S=\frac{5}{2}$. We have also the equation

$$|J| = g^2\beta^2/2Z\chi_1, \quad (7)$$

which relates $|J|$ to χ_1 , the perpendicular susceptibility of an antiferromagnet (per iron ion for $t < 1$). Here, g is the g factor (taken as 2) and β is the Bohr magneton.

The values of $|J|$ derived from (4) and the measured values of T_N are given in Table III for all the orthoferrites. In the same table are given the values of $|J|$ derived from (7) and the experimental values of χ_1 . Since χ_1 in (7) is only the susceptibility of the mag-

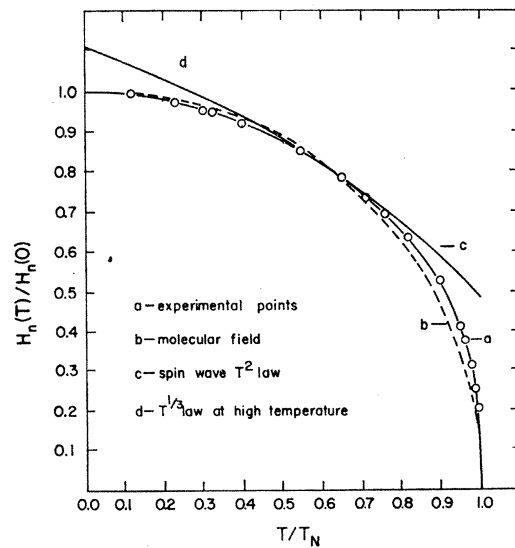


FIG. 8. Internal magnetic field $H_n(T)/H_n(0)$ as a function of the reduced temperature $t = T/T_N$ for LaFeO_3 . (a) Experimentally (the circles are the experimental points) and theoretically; (b) molecular-field approximation for $S=\frac{5}{2}$; (c) spin-wave T^2 law at low temperature; (d) $T^{1/3}$ law at high temperature.

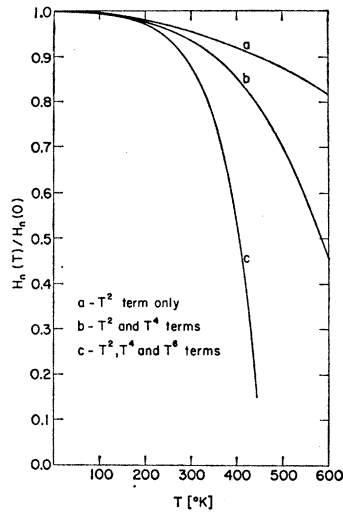


FIG. 9. The iron sublattice magnetization $H_n(T)/H_n(0)$, theoretically, after Oguchi's spin-wave theory, as a function of temperature.

netically ordered iron ions, it could be measured only in materials where R is diamagnetic. The measurements of χ_1 had to be performed on single crystals and, since LaFeO_3 is almost cubic, all the crystals were twinned and χ_1 could not be measured. Agreement between the values of $|J|$, from measurements of T_N of χ_1 , is poor. The value of $|J|$ calculated from the experimental values of the high-temperature susceptibility²⁷ are also given in Table III.

The broken line in Fig. 8 is a plot of the reduced sublattice magnetizations versus reduced temperature t calculated from (6). The experimental curve for LaFeO_3 is given for comparison. The experimental curve for LaFeO_3 , as for all the other orthoferrites, is below the theoretical curve in the range $0 < t < 0.5$ and above it in the range $0.5 < t < 1$. A similar situation was found in $\alpha\text{Fe}_2\text{O}_3$.²⁸

D. High-Temperature Series Expansion

This theory expands the susceptibility above T_N in a series of inverse powers of the reduced temperature t . The Néel temperature is defined as the singular point in this expansion, as estimated by Padé extrapolation from the first few terms of the series. For a simple cubic antiferromagnet, the relation between $|J|$ and T_N is given by²⁹

$$T_N = \frac{5|J|}{192k} (Z-1)[11S(S+1)-1] \times [1+0.63/ZS(S+1)], \quad (8)$$

which, for $S = \frac{5}{2}$ and $Z = 6$, reduces to

$$T_N = 12.55|J|k^{-1}. \quad (9)$$

The values of $|J|$ derived from this equation are given in Table III.

E. Spin-Wave Theory

Kubo,³⁰ and subsequently Oguchi, have calculated the sublattice magnetization in terms of a series expansion in powers of $kT/|J|$. The Kubo result, or "simple spin-wave theory," provides the first non-vanishing temperature-dependent term ($\sim T^2$), whereas the Oguchi corrections give terms of order T^4 and T^6 . For a simple cubic antiferromagnet with negligible anisotropy, Kubo's³⁰ and Oguchi's³¹ results are

$$\frac{\sigma_s(T)}{\sigma_s(0)} = 1 - 1.590 \frac{k^2 T^2}{J^2}, \quad (10)$$

$$\frac{\sigma_s(T)}{\sigma_s(0)} = 1 - 1.528 \times 10^{-3} \frac{k^2 T^2}{J^2} - 2.572 \times 10^{-5} \frac{k^4 T^4}{J^4} - 2.007 \times 10^{-6} \frac{k^6 T^6}{J^6}. \quad (11)$$

Plotting the experimental magnetization $\sigma_s(T)/\sigma_s(0)$ as a function of T^2 , we calculated from the slope of this curve and Eq. (10) the exchange integral $|J|$. The values of $|J|k^{-1}$ deduced from Kubo's spin-wave theory²⁸ [Eq. (10)] are given in Table III. These values are nearly equal to the values calculated from molecular-field theory. A good fit was obtained to the experimental curve in a wide range of temperature up to $T/T_N < 0.6$ using Kubo's spin-wave theory [Eq. (10)] with $|J|k^{-1} = 39^\circ\text{K}$ for the case of LaFeO_3 (see Fig. 8).

In Fig. 9, we have plotted the sum of the terms to order T^2 , to order T^4 , and to order T^6 from Eq. (11) for a $|J|k^{-1} = 55^\circ\text{K}$. We find that the simple spin-wave theory ($\sim T^2$) is reliable up to $T/T_N \sim 0.3$, the Oguchi correction terms being negligible below this temperature. There is no temperature region in which the Oguchi correction terms appear to be convergent (i.e., in which the corrections are small compared to the T^4 corrections, etc.). Thus the agreement between the Kubo's results and the experiment over such a wide temperature range, as shown in Fig. 8, should be regarded as fortuitous, as should the agreement between the Kubo exchange and the molecular-field exchange. We have tried to compare Oguchi's series with the experimental results. In Fig. 10, we plot the sublattice magnetization versus T_N for various exchange integrals, and the experimental results for LaFeO_3 . Although only a single experimental point provides a discrimination among various curves, the most plausible value of J for LaFeO_3 is found to be

$$|J|k^{-1} = (58 \pm 5)^\circ\text{K}.$$

²⁷ G. Gorodetsky (private communication).

²⁸ K. Ono and A. Ito, J. Phys. Soc. Japan **17**, 1012 (1960).

²⁹ G. S. Rushbrook and P. J. Wood, Mol. Phys. **6**, 409 (1963).

³⁰ R. Kubo, Phys. Rev. **87**, 568 (1952).

³¹ T. Oguchi, Phys. Rev. **117**, 123 (1960).

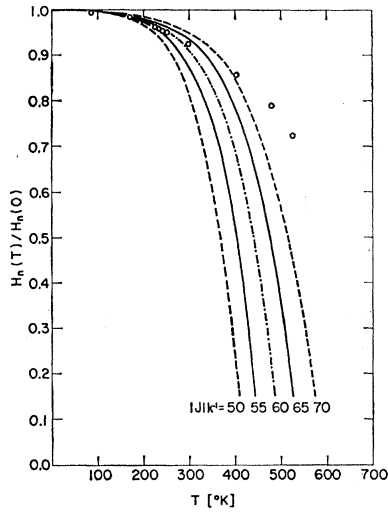


FIG. 10. Theoretical sublattice magnetization $H_n(T)/H_n(0)$, after Oguchi's spin-wave theory, and different exchange integrals as a function of temperature. The points are the experimental results.

It is gratifying to note that this value is in good agreement with the value obtained from other measurements (see Table III). Equation (11) fits the experimental results for LaFeO_3 for a $|J|k^{-1}=58^\circ\text{K}$ (see Fig. 10); we concluded that the exchange integral is practically equal to that calculated from the high-temperature expansion. The values of $|J|k^{-1}$ deduced from Oguchi's spin-wave theory which give the best fit for Eq. (11) to the experimental curve are also given in Table III. The internal field at 0°K was calculated from Eq. (11) by extrapolation and for a $|J|k^{-1}$ giving the best fit to the experimental curve. The values are found to be about 0.5% higher than at 85°K . The internal-field results for all the orthoferrites at 0°K are given in Fig. 11. Note that $H_n(0)$ depends on the crystallographic environment, which is different for different R ions.

F. Green's-Function Theory

The reduced sublattice magnetization $\langle S_z \rangle / S$ as a function of temperature of a Heisenberg antiferromagnet in the random-phase approximation (RPA) and Callen decoupling (CD) cases was calculated by Anderson and Callen³² using Green's-function equations. For zero anisotropy, $\langle S^z \rangle$ is given by¹²

$$\langle S^z \rangle = \left\{ \left[S + \frac{1}{2} - \Omega(0) \right] \left[\Omega(0) + \frac{1}{2} \right]^{2S+1} + \left[S + \frac{1}{2} + \Omega(0) \right] \left[\Omega(0) - \frac{1}{2} \right]^{2S+1} \right\} \times \left\{ \left[\Omega(0) + \frac{1}{2} \right]^{2S+1} - \left[\Omega(0) - \frac{1}{2} \right]^{2S+1} \right\}^{-1}, \quad (12)$$

where

$$\Omega(R) = \frac{2}{N} \sum_k e^{ik \cdot R} (1 - \ell^2 \gamma_k^2)^{-1/2} \times \left\{ \left[e^{\beta b} (1 - \ell^2 \gamma_k^2)^{1/2} - 1 \right]^{-1} + \frac{1}{2} \right\}. \quad (13)$$

$R = \delta - \delta'$ are the nearest-neighbor vectors and, for a

simple cubic lattice, γ_k is given by

$$\gamma_k = \frac{1}{3} (\cos k_x a + \cos k_y a + \cos k_z a), \quad (14)$$

where a is the lattice constant, k_x , k_y , and k_z are vectors in the directions x , y , and z , respectively, $\beta = 1/k_B T$, and b is given by the equation which also gives the relation between the sublattice magnetization and the temperature,

$$k_B T = \frac{zJ \langle S^z \rangle}{\beta b} \left[1 + 2\alpha \langle S^z \rangle - \frac{1}{z} \sum_{\delta'} \Omega(\delta - \delta') \right]. \quad (15)$$

Here, the summation δ' extends over the z nearest-neighbor vectors. In the random-phase approximation, $\alpha = 0$, and in the decoupling scheme proposed by Callen (CD), $\alpha = 1/2S^2$. If we take βb as a parameter, we thereby determine $\Omega(0)$ and $\Omega(R)$ from (13), the sublattice magnetization from (12), and the temperature from (15).

The numerical calculation of the sublattice magnetization has been programmed for our CDC 1604 computer. The computer program³³ calculates $\Omega(0)$, $\Omega(R)$, $\langle S^z \rangle$, and T/T_N as a function of the parameter βb . The results are given in Fig. 12. In the same Fig. 12, we give the numerical calculation of the sublattice magnetization as a function of temperature if we use Copeland-Gersch³⁴ coupling, i.e., $\alpha = \langle S^z \rangle^2 / 2S^4$ in place of $\alpha = 1/2S^2$ for CD (see Fig. 12, curve C.G).

We observe that the CD is good at low temperature up to about $0.5 T/T_N$. Note that the over-all disagreement between theory and experiment in Fig. 12 is not very different for the Green's-function theories and the molecular-field theory.

It should be remembered, however, that the results are given in this figure in reduced coordinates. As can be seen from Table III, the molecular-field exchange constant is considerably smaller than the exchange given by the better estimates (rows 3-7, Table III). Thus, the molecular-field result, if plotted with the temperature and not the reduced temperature as the

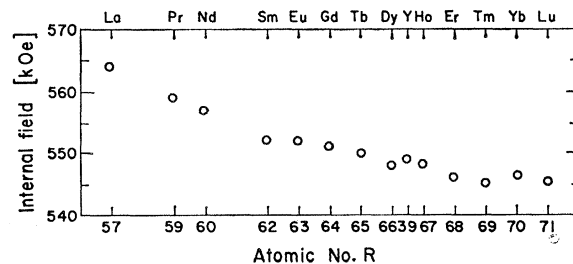


FIG. 11. Internal field at zero $^\circ\text{K}$ as a function of atomic rare-earth number R .

³³ Integrals were evaluated by three-dimensional Gaussian quadrature, using a program kindly supplied by Professor P. Rabinowitz.

³⁴ J. A. Copeland and H. A. Gersch, Phys. Rev. 143, 236 (1966).

³² F. B. Anderson and H. B. Callen, Phys. Rev. 136, A1068 (1964).

TABLE IV. Theoretical and experimental values for β and D .

	β	Range T/T_c	D	References
Theory				
Molecular field	$\frac{1}{2}$	$T \rightarrow T_c$	1.441	39
Landau's theory of second-order phase transition	$\frac{1}{2}$	$T \rightarrow T_c$		35
Two-dimensional Ising models	$\frac{1}{2}$	$T \rightarrow T_c$	1.2 -1.26	36, 37
Three-dimensional Ising model	$\frac{1}{2}$	$T \rightarrow T_c$	1.48-1.57	37, 38
Green's function RPA	$\frac{5}{6} \pm 0.007$	$0.54 < T/T_c < 0.86$	1.11	39
Green's function CD	$\frac{1}{2}$	$0.54 < T/T_c < 0.86$	1.09	39
Green's function	$\frac{1}{2}$	$T \rightarrow T_c$		39
Two-spin cluster theory	$\frac{1}{2}$	$0.73 < T/T_c < 0.88$	1.124	39
Two-spin cluster theory	$\frac{1}{2}$	$T \rightarrow T_c$		39
Experiment				
MnF ₂	0.333 ± 0.003	$0.97 < T/T_N < 0.9999$	1.2	40, 44
EuS	0.33 ± 0.015	$0.87 < T/T_c < 0.99$	1.145 ± 0.02	41, 44
Fe ⁵⁷ in Ni	0.33 ± 0.03	$0.84 < T/T_c < 0.99$		42
Fe ⁵⁷ in Ni	0.51 ± 0.04	$0.996 < T/T_c < 0.9995$		42
Fe ⁵⁷ in Fe metal	0.33 ± 0.005	$0.80 < T/T_c < 0.996$	1.32 ± 0.02	43
Fe ⁵⁷ in RFeO ₃	0.348 ± 0.005	$0.60 < T/T_N < 0.99$	1.14 ± 0.02	45
Fe ⁵⁷ in YFeO ₃	0.55 ± 0.04	$0.996 < T/T_N < 1.003$	3.9	46

abscissa, would disagree with experiment considerably more than any of the Green's-function theories.

G. Critical Behavior

The relative sublattice magnetization as a function of temperature T near the Néel point has been found both in various theories³⁵⁻³⁹ and experimentally⁴⁰⁻⁴⁷ to follow the equation

$$\frac{\sigma_s(T)}{\sigma_s(0)} = D \left(1 - \frac{T}{T_N}\right)^\beta, \quad (16)$$

where $\sigma_s(T)$ is the sublattice magnetization at a given temperature and T_N is the Néel temperature. Different values of β have been reported in the literature. A summary of the present situation is given in Table IV.

In Fig. 13, the internal field $H_n(T)/H_n(0)$ versus $(1 - T/T_N)$ is plotted on a double logarithmic scale. These plots are straight lines in the range $0.60 < T/T_N < 0.99$. Here, the upper bound is determined by the resolution of the spectra in the experiment (see Fig. 3).

The exponent β and the coefficient D obtained from

TABLE V. Values of β and D in orthoferrites.

R	β	D	Range T/T_N	
			min	max
La	0.347	1.11	0.60	0.993
Pr	0.345	1.12	0.55	0.996
Nd	0.353	1.14	0.70	0.993
Sm	0.342	1.13	0.60	0.990
Eu	0.350	1.17	0.65	0.985
Gd	0.354	1.15	0.70	0.980
Tb	0.349	1.12	0.55	0.990
Dy	0.348	1.14	0.65	0.990
Y	0.354	1.16	0.70	0.975
Ho	0.342	1.15	0.60	0.980
Er	0.357	1.15	0.70	0.980
Tm	0.349	1.15	0.65	0.990
Yb	0.339	1.13	0.60	0.993
Lu	0.342	1.17	0.65	0.997

the logarithmic plots are given in Table V. The error in β is ± 0.005 , and in D it is ± 0.02 . We find that, on the average, $\beta = 0.348$; it is thus quite close to $\frac{1}{3}$. The error in the determination of β comes from the experimental uncertainties in the measurements of the temperature and the internal field.

³⁵ L. D. Landau and E. M. Lifschitz, *Statistical Physics* (Pergamon Press, Inc., New York, 1958).

³⁶ C. N. Yang, *Phys. Rev.* **85**, 808 (1952).

³⁷ G. A. Baker, Jr., *Phys. Rev.* **124**, 768 (1961).

³⁸ J. W. Essam and M. F. Fisher, *J. Chem. Phys.* **38**, 802 (1963).

³⁹ E. Callen and H. B. Callen, *J. Appl. Phys.* **36**, 1140 (1965).

⁴⁰ P. Heller and G. Benedek, *Phys. Rev. Letters* **8**, 428 (1962).

⁴¹ P. Heller and G. Benedek, *Phys. Rev. Letters* **14**, 71 (1965).

⁴² D. G. Howard, B. D. Dunlap, and J. G. Dash, *Phys. Rev. Letters* **15**, 628 (1965).

⁴³ R. S. Preston, S. S. Hanna, and J. Heberle, *Phys. Rev.* **128**, 2207 (1962).

⁴⁴ P. Heller and G. B. Benedek, in *Proceedings of the International Conference on Magnetism, Nottingham, 1964* (The Institute of Physics and The Physical Society, London, 1965), p. 97.

⁴⁵ M. Eibschütz, S. Shtrikman, and D. Treves, *Solid State Commun.* **4**, 141 (1966).

⁴⁶ G. Gorodetsky, S. Shtrikman, and D. Treves, *Solid State Commun.* **4**, 147 (1966).

⁴⁷ M. E. Fisher, *J. Math. Phys. (N. Y.)* **5**, 944 (1964).

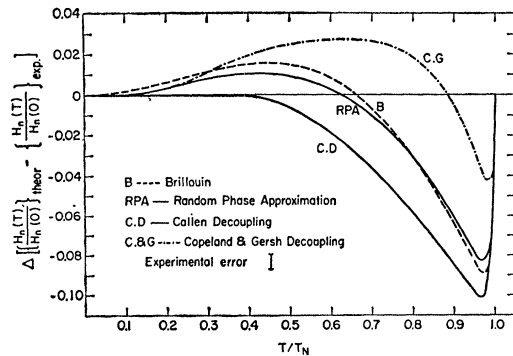


FIG. 12. The difference between various theoretical and experimental internal-field results as a function of reduced temperature for LaFeO₃.

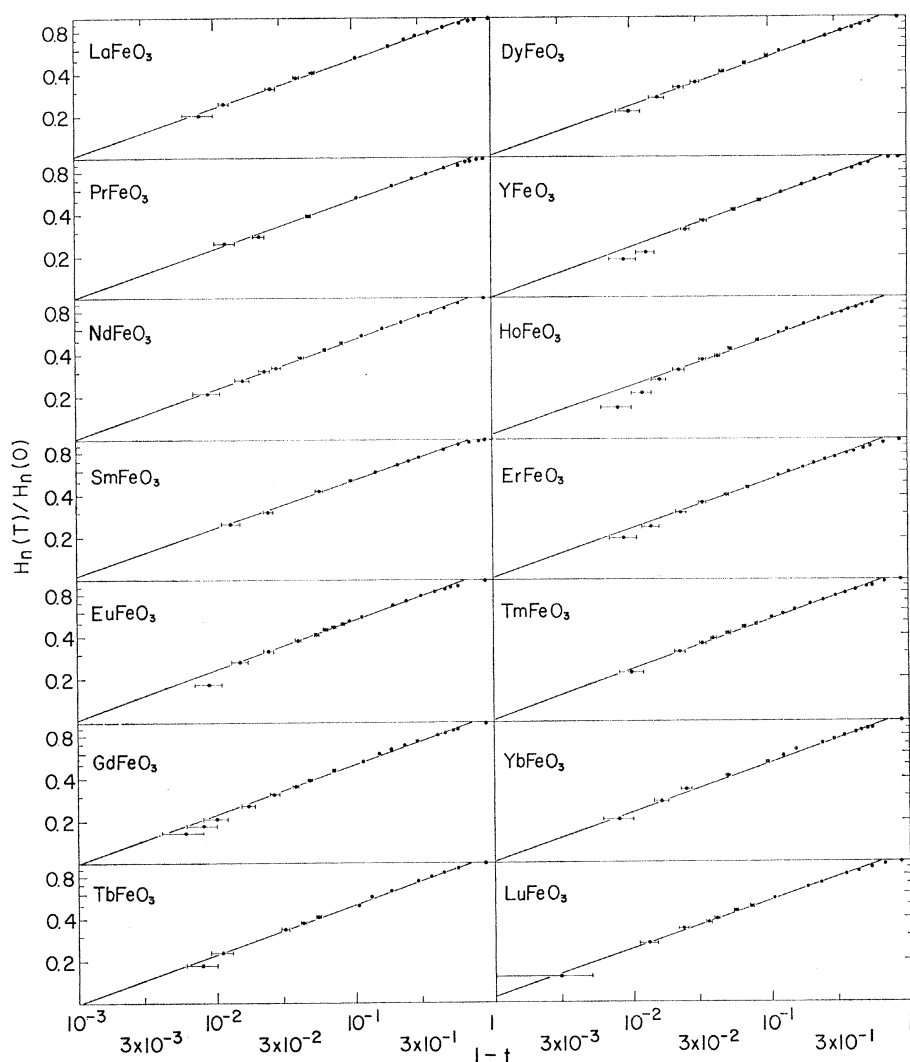


FIG. 13. Internal field $H_n(T)/H_n(0)$ of orthoferrites as a function of $1-t$, where $t=T/T_N$.

We have also tried to determine β following the method of Heller and Benedek,⁴¹ namely, by plotting

$$\frac{\Delta T}{T_N} = \frac{(T_N - T)}{T_N} = \frac{1}{D} \left\{ \frac{H_n(T)}{H_n(0)} \right\}^{1/\beta} \quad (17)$$

versus T/T_N for various β . The curves for LaFeO_3 are shown in Fig. 14. Equation (16) holds in the region where the curve from Fig. 14 has no curvature. Figure 14 shows that the data are in good agreement with Eq. (16) for LaFeO_3 in the range of temperature $0.60T_N < T < 0.993T_N$ for $\beta = 0.33$. [It is interesting to note that if we take internal field as a function of temperature for iron metal from Preston *et al.*,⁴³ we also find that the one-third law holds in the range $0.80 < T/T_c < 0.996$ (T_c is the Curie temperature).]

We thus conclude that the dependence of the internal field in orthoferrites in the range $0.60T_N < T < 0.99T_N$ follows relations (16) with a value of β close to $\frac{1}{3}$.

H. The Quadrupole Coupling

The measured value of the quadrupole coupling constant ϵ for all the orthoferrites as a function of temperature is given in Table II. This interaction is proportional to the electric-field gradient tensor V_{ij} at the site of the Fe^{57} nucleus, and thus reflects the crystalline structure. Below T_N , the quadrupole interaction is a small perturbation on the magnetic nuclear-energy levels, and to first order is given by⁴⁸

$$\epsilon = -3eQV_{ii}^H/4I(2I-1). \quad (18)$$

Here, e is the electron charge and Q is the nuclear quadrupole moment of the first excited state which has a nuclear spin $I = \frac{3}{2}$. For Fe^{57} , the value of⁴⁹ $Q = 0.41$ b was taken. V_{ii}^H is the electric-field gradient com-

⁴⁸ Reviews of the nuclear coupling can be found in the following references: M. H. Cohen and I. Reif, *Solid State Phys.* **5**, 321 (1957); J. P. Das and E. L. Hahn, *Solid State Phys., Suppl.* **1**, 3 (1958).

⁴⁹ J. O. Artman, *Phys. Rev.* **143**, 541 (1966).

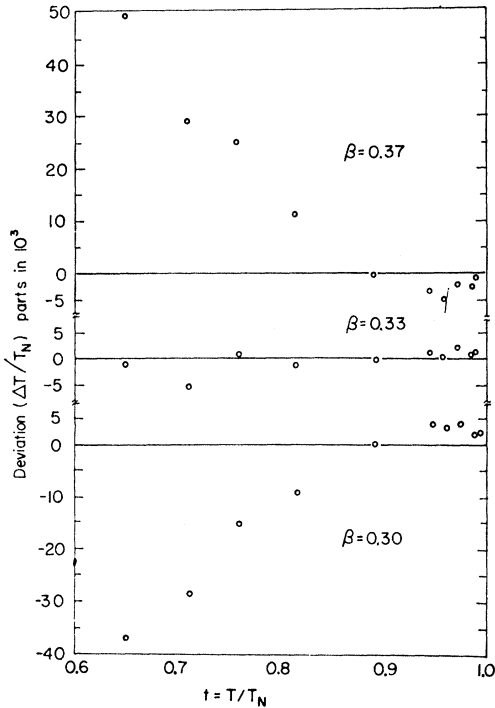


FIG. 14. Deviation from Eq. (16) for three choices of β for LaFeO_3 . The most appropriate choice is the one for which the plot $\Delta T/T_n$ versus T/T_N has no curvature as $T \rightarrow T_N$.

ponent in the direction of quantization of the nuclear moment, i.e., the direction of the internal field or the sublattice magnetization. In the orthoferrites, i is, to a very good approximation (see Table I), either in the x or z crystallographic direction, depending on R and the temperature.⁷

For YFeO_3 and GdFeO_3 , the position of all the ions in the crystal at room temperature is known.² Thus V_{ii}^H could be calculated and a comparison made between the measured values and those calculated from (18). In both materials, $i=x$. V_{xx}^H was calculated by a single-point charge lattice sum⁵⁰ which gives

$$V_{xx}^H = (1 - \gamma_\infty) \left[\sum_n \frac{\rho_n}{|r_n|^3} \left(\frac{3r_{nx}^2}{r_n^2} - 1 \right) \right]. \quad (19)$$

Here, ρ_n is the charge of the n th ion, r_n its distance from the nucleus at which the gradient is calculated (which is taken as the origin of the coordinate system), and r_{nx} is the component of r_n in the direction of quantization. The sum was taken over all ions except the one at the origin and was carried out on a CDC 1604 computer. Additional shells of ions, each one unit cell thick, were added in the sum until the correction of an additional shell was negligible. γ_∞ is the Stern-

⁵⁰ G. K. Wertheim, *Mössbauer Effect* (Academic Press Inc., New York, 1964), p. 15.

TABLE VI. The quadrupole coupling constant, both experimental and calculated, for GdFeO_3 and YFeO_3 .

Materials	Experimental results		Calculated results	Temperature
	ϵ (mm/sec)	ϵ (kc/sec)	ϵ (kc/sec)	
GdFeO_3	0.03 ± 0.01	330 ± 110	300 ± 170	room
			1550	$> T_N$
YFeO_3	0.01 ± 0.01	110 ± 110	9 ± 23	room
			510	$> T_N$

heimer antishielding factor⁵¹ which represents the contribution to V_{ij} due to the polarization of the electronic cloud of the Fe^{3+} ion at the origin by the electric field of all the other ions. The value⁵² $\gamma_\infty = -9.14$ was used in the calculation. The measured and calculated values are compared in Table VI.

Chappert⁵³ observed that, at the temperature of 680°C , the Mössbauer spectrum of YFeO_3 shows a quadrupole splitting. We observed, at high temperature, a broadening of the resonance line of approximately 20%, but did not see a definite quadrupole splitting in the spectrum. Our numerical calculation shows that the off-diagonal elements of the field-gradient tensor cannot be neglected. Diagonalizing this tensor, we get its eigenvalues and, consequently, the quadrupole coupling in the paramagnetic state using the crystallo-

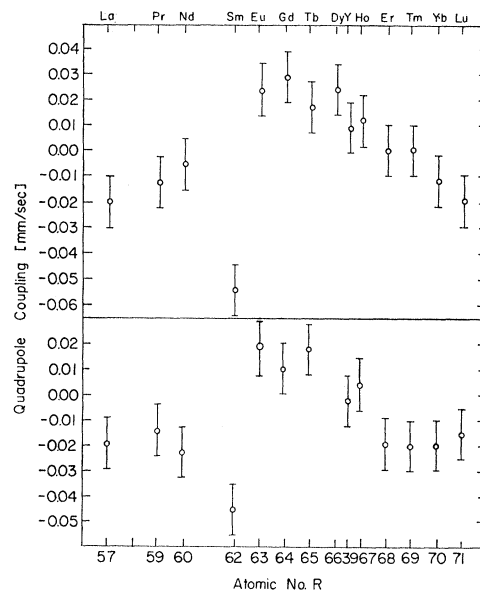


FIG. 15. The quadrupole coupling constant as a function of the atomic number R . (a) At room temperature and (b) at liquid-air temperature.

⁵¹ R. M. Sternheimer and H. M. Foley, *Phys. Rev.* **102**, 731 (1956); R. M. Sternheimer, *ibid.* **84**, 244 (1951); **86**, 316 (1952); **95**, 736 (1954).

⁵² G. Burns and E. G. Wikner, *Phys. Rev.* **121**, 155 (1961); R. M. Sternheimer, *ibid.* **130**, 1423 (1963).

⁵³ J. Chappert (private communication).

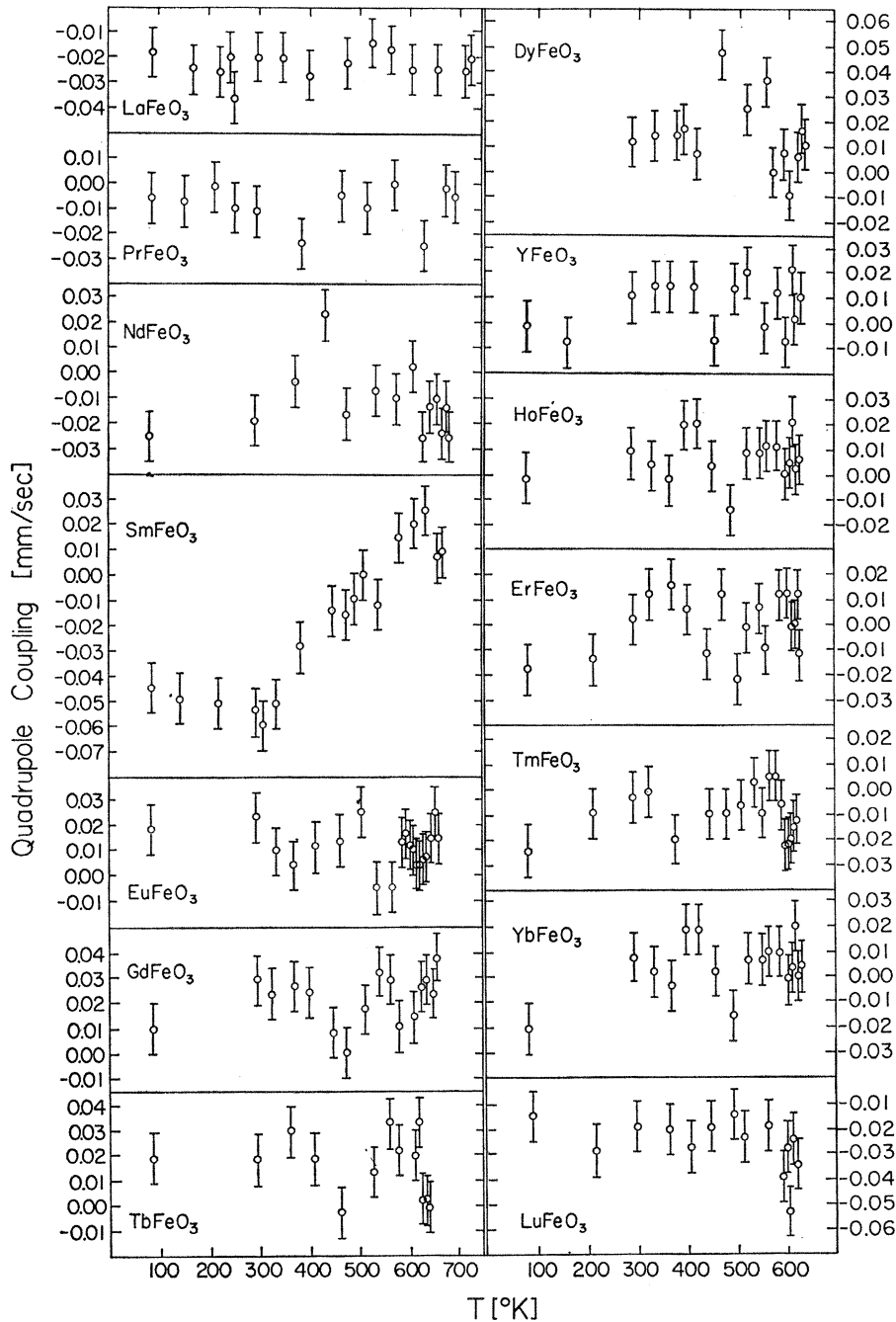


FIG. 16. The quadrupole coupling constant versus temperature in orthoferrites.

graphic data available at room temperature (see Table VI).

Figure 15 shows that ϵ at room temperature varies regularly with R , while at 85°K it is essentially constant. SmFeO_3 is an exception, both in its ϵ value and in the fact that it is the only orthoferrite in which $i=z$ at room temperature.⁷ It is interesting to note (see Fig. 16) that ϵ for SmFeO_3 rises smoothly between 300 and 600°K, and goes through zero at about 480°K, which coincides with the temperature at which i goes from z

to x . However, this transition is rather abrupt, and occurs over a temperature range²⁷ of 30°K.

This correlation of the quadrupole coupling constant with the direction of antiferromagnetism, which is to be expected, seems not to be limited to the case of SmFeO_3 . In NdFeO_3 , ErFeO_3 , and TmFeO_3 , a change in the direction of antiferromagnetism from the x to z as the temperature is lowered occurs around the liquid-nitrogen temperature. As can be seen, a similar, though less-marked, trend in the temperature dependence of

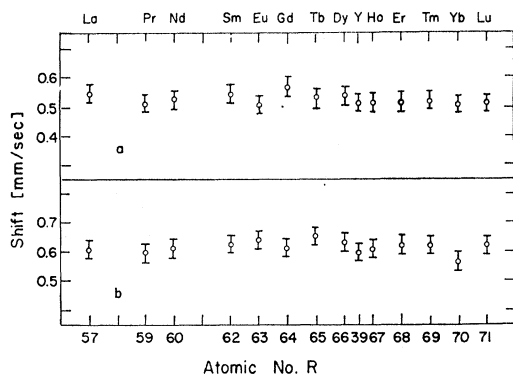


FIG. 17. This shift in the spectrum of Fe^{57} of orthoferrites as a function of atomic number R . (a) At room temperature and (b) at liquid-air temperature.

the quadrupole coupling seems to exist in these compounds at the above temperatures.

I. The Isomer Shift

The shift ΔE of the center of gravity of the spectra, as given in Fig. 17, is essentially the same for all the orthoferrites. It is 0.51 ± 0.03 mm/sec at 296°K and 0.61 ± 0.03 mm/sec at 85°K with respect to the chromium source.

The position of the center of gravity is determined by the isomer shift and the temperature shift.⁵⁴ It is here assumed that the isomer shift is temperature-independent, and that it is equal to the shift of the center of gravity at 85°K, where the temperature shift is negligible (see the next paragraph). The value 0.61 mm/sec for the isomer shift with respect to Cr is in very good agreement with that expected for the $3d^5$ configuration⁵⁵ appropriate to the Fe^{3+} ion.

J. The Temperature Shift

Figure 18 shows the temperature dependence of ΔE for the orthoferrites. Subtracting the isomer shift from ΔE , one gets the temperature shift which is proportional to the Fe^{57} nuclear vibrational energy. The temperature coefficient $(1/\nu)(\partial\nu/\partial T)_p$ calculated from the slope of the temperature shift for all the orthoferrites, is given in Table VII. Thus the slopes of the curves of Fig. 18 are proportional to the Fe^{57} nuclear specific heat C_p . At low temperatures, the slope is essentially zero, thereby justifying our neglect of the temperature shift as given in Table VII. Using the relation⁵⁴ for harmonic lattice forces

$$C_p = -\frac{1}{\nu} \left(\frac{\partial \nu}{\partial T} \right)_p 2Mc^2 \frac{\text{erg}}{\text{mole deg}}, \quad (20)$$

⁵⁴ H. Fraunfelder, *The Mössbauer Effect* (W. A. Benjamin, Inc., New York, 1962); A. J. Boyle and H. E. Hall, *Rept. Progr. Phys.* **25**, 441 (1962).

⁵⁵ L. R. Walker, G. K. Wertheim, and V. Jaccarino, *Phys. Rev. Letters* **6**, 98 (1961).

TABLE VII. Temperature coefficients and specific heat in orthoferrites derived from the temperature coefficients using Eq. (20).

$R\text{FeO}_3$	T (K°)	$\frac{1}{\nu} \left(\frac{\partial \nu}{\partial T} \right)_p$ ($\times 10^{+16}$)	$C_p(\text{Fe})$ (cal/mole deg)
La	100-730	-2.46	5.99
Pr	300-645	-2.71	6.61
Nd	300-690	-2.30	5.59
Sm	300-573	-2.54	6.21
Eu	300-616	-2.50	6.10
Gd	300-617	-2.70	6.61
Tb	300-602	-2.54	6.21
Dy	300-562	-2.42	5.93
Y	325-615	-2.71	6.61
Ho	325-597	-2.67	6.50
Er	300-590	-2.71	6.61
Tm	300-598	-2.53	6.16
Yb	300-594	-2.47	6.04
Lu	300-585	-2.25	5.47
Error		± 0.3	± 0.63

one gets the specific heat of the iron nuclei. Here, M is the nuclear weight of Fe^{57} , c is the velocity of light in cm/sec, and ν is the frequency of the γ ray. The calculated values of C_p are given in Table VII. They compare reasonably well with the expected value of 6 cal/mole deg.

In Fig. 19 are given theoretical plots of the vibrational energy as a function of temperature for the

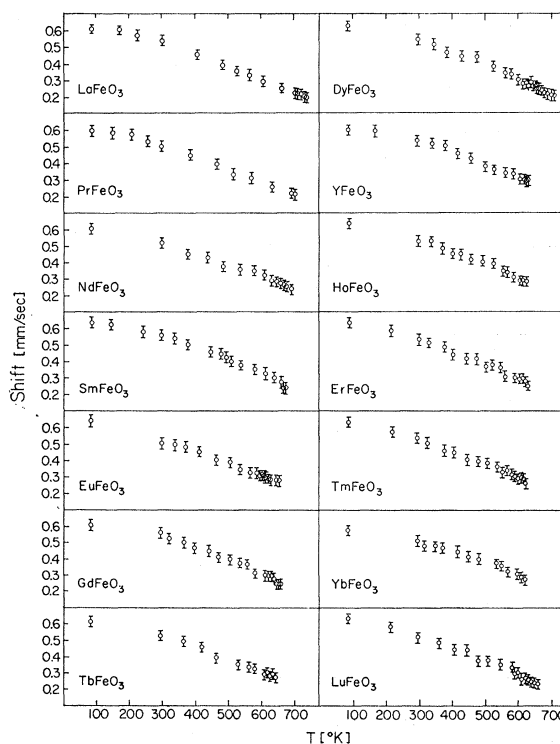


FIG. 18. The shift in the spectrum of Fe^{57} of orthoferrites versus temperature.

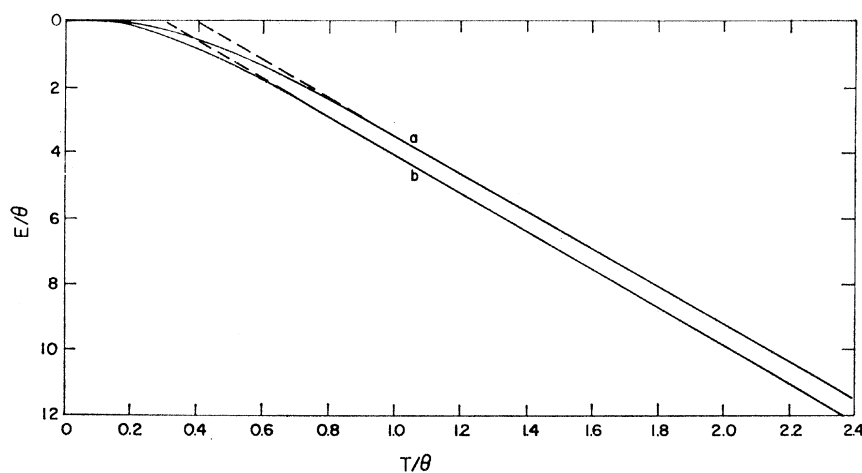


FIG. 19. The internal energy E/Θ as a function of temperature T/Θ . (a) Einstein model and (b) Debye model. (Θ is the characteristic temperature.)

Einstein and Debye model.⁵⁶ The intercept of the high-temperature asymptotes with the $E=0$ level defines the cutoff temperature. One finds that $\Theta_E=2.5T_i$ and $\Theta_D=3.3T_i$ where T_i is the intercept temperature and Θ_E , Θ_D are the Einstein and Debye temperatures, respectively. Using Fig. 19, and identifying the $E=0$ level with the low-temperature value of ΔE , one gets T_i and thus Θ_E and Θ_D . The results are summarized in Table VIII. When using these results, one should of course recall that a drastic approximation has been made by using an Einstein or Debye model for the orthoferrites.

K. The Mössbauer Fraction

The data of Fig. 18 are not accurate enough to enable a distinction between the Einstein and Debye models. However, the measurement of the temperature dependence of the Mössbauer fraction f supplied additional information that may be used to distinguish

TABLE VIII. Einstein characteristic temperature Θ_E and Debye characteristic temperature Θ_D in the orthoferrites.

R	T	Θ_E	Θ_D
La	240	600	800
Pr	235	590	780
Nd	230	575	770
Sm	220	550	730
Eu	220	550	730
Gd	230	575	770
Tb	220	550	730
Dy	205	500	680
Y	240	600	800
Ho	220	550	730
Er	205	500	680
Tm	200	500	670
Yb	230	575	770
Lu	200	500	670
Average		550	735

⁵⁶ Here we ignore the differences in position and mass of different ions in the orthoferrites. See, for example, J. M. Ziman, *Principles of the Theory of Solids* (Cambridge University Press, London, 1964).

between these two models. For the Einstein model f , is given by^{56,57}

$$f = \exp\left(-\frac{E_R}{k\Theta_E} \coth\frac{\Theta_E}{2T}\right), \quad (21)$$

while for the Debye model^{56,58}

$$f = \exp\left\{-\frac{3}{2} \frac{E_R}{k\Theta_D} \left[1 + 4 \left(\frac{T}{\Theta_D}\right)^2 \int_0^{\Theta_D/T} \frac{x}{e^x - 1} dx\right]\right\}. \quad (22)$$

Here, k is Boltzmann's constant and $E_R=0.002$ eV is the recoil energy of the free Fe^{57} nucleus. The solid lines of Fig. 20 are obtained from Eqs. (21) and (22) for different values of cutoff temperatures.

The Mössbauer fraction was measured for YFeO_3 . An unenriched absorber having 10 mg/cm² was used. This absorber has 0.06 mg/cm² Fe^{57} and is thus a thin absorber, as natural iron contains 2.17% Fe^{57} . Spectra were taken between 85 and 720°K. The ratio of the absorption peaks was 1:2:3, appropriate to a thin absorber.⁵⁹ The temperature dependence of the area of the absorption peaks, which is proportional to the Mössbauer fraction,⁶⁰ was fitted to the theoretical curves of Fig. 20. The experimental points fit the curves for $\Theta_E=300^\circ\text{K}$ and $\Theta_D=800 \pm 50^\circ\text{K}$ well. From Table VIII, one finds that the temperature shift yielded $\Theta_E=600^\circ\text{K}$

⁵⁷ R. H. Herber and G. K. Wertheim, in *Proceedings of the Second International Conference on the Mössbauer Effect, Saclay, France, 1961*, edited by A. H. Schoen and D. M. J. Compton (John Wiley & Sons, Inc., New York, 1962), p. 105.

⁵⁸ R. L. Mössbauer and W. H. Wiedemann, *Z. Physik* **159**, 33 (1960); H. J. Lipkin, *Ann. Phys. (N. Y.)* **9**, 332 (1960); **18**, 182 (1960); W. M. Visscher, *ibid.* **9**, 194 (1960); J. Petzold, *Z. Physik* **163**, 71 (1961); Singwi and A. Sjolander, *Phys. Rev.* **120**, 1093 (1960); B. Kaufmann and H. J. Lipkin, *Ann. Phys. (N. Y.)* **18**, 294 (1962).

⁵⁹ O. C. Kistner and A. W. Sunjar, *Phys. Rev. Letters* **4**, 412 (1960).

⁶⁰ S. Margulies and J. R. Ehrman, *Nucl. Instr. Methods* **12**, 131 (1961); S. Margulies, P. Debruner, and H. Fraunfelder, *ibid.* **21**, 217 (1963); D. A. O'Connor, *ibid.* **21**, 318 (1963); G. Lang, *ibid.* **24**, 425 (1963).

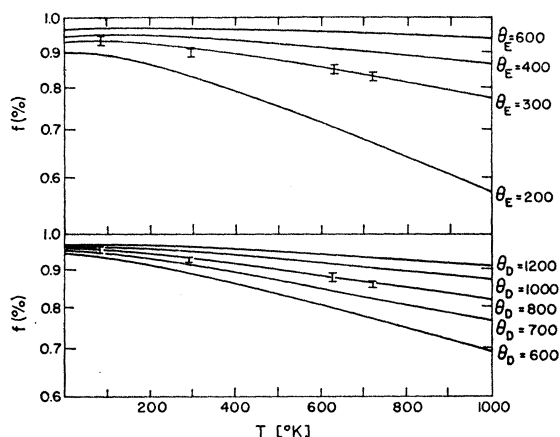


FIG. 20. Mössbauer fraction theoretically as a function of temperature for different characteristic temperatures: (a) Einstein temperature Θ_E and (b) Debye temperature Θ_D . The points are the experimental results.

and $\Theta_D = 800^\circ\text{K}$. Thus, from a comparison of these two measurements, one may conclude that the Debye model gives more consistent results. This model and $\Theta_D = 800^\circ\text{K}$ result in $f = 96\%$ at $T = 0^\circ\text{K}$.

IV. CONCLUSIONS

From the study of the hyperfine interaction in orthoferrites in the work above, the following conclusions were drawn:

1. The Mössbauer effect of Fe^{57} in $R\text{FeO}_3$ from liquid-air temperature to the Néel temperature shows a characteristic six-line pattern, indicating that all the iron atoms are in equivalent sites, in agreement with the crystallographic structure of these materials.
2. The internal field at the iron nucleus does not result only from the iron ion, but is also influenced by the environment. The internal field at 0°K decreases regularly with the atomic number R from (564 ± 2) kOe for LaFeO_3 to (545.5 ± 2) kOe for LuFeO_3 .
3. The behavior of the internal magnetic field as a function of temperature is similar to that of the net (weak ferromagnetic) magnetization as a function of temperature. There is a linear relation between them up to the Néel temperature. The canting angle α is essentially constant over the entire temperature region. This angle was found to be between 8 and 11 mrad.
4. The internal field as a function of temperature is not in good agreement with the sublattice magnetization calculated from the molecular-field approximation. The sublattice magnetization calculated from the Brillouin function is slightly greater than the experimental value at low temperature. There is increasing deviation in the neighborhood of the Néel temperature, where the theoretical curve falls more rapidly.
5. The exchange integral calculated from Oguchi's spin-wave theory is in good agreement with that cal-

culated from Rushbrook and Wood's relation for the Néel temperature. The range of $|J|k^{-1}$ is from 58.0°K for LaFeO_3 to 50.0°K for LuFeO_3 . The value of the exchange integral calculated from the expression for the Néel temperature from the molecular-field approximation is small and incorrect, as expected.

6. Of the different Green's-function theories of the Heisenberg antiferromagnet—RPA, CD, and the Copeland-Gersh theory—the CD theory best describes the temperature dependence of the sublattice magnetization at low temperature. All the theories fail for $T/T_N > 0.50$.

7. The Néel temperature T_N decreases smoothly with the atomic number R from 740°K for LaFeO_3 to 623°K for LuFeO_3 . The average exchange integral for the iron ion and the Néel temperature are approximately proportional to the cosine of the superexchange angle $\text{Fe}^{3+}-\text{O}^{2-}-\text{Fe}^{3+}$.

8. A good agreement was obtained between the experimental and calculated results for the quadrupole coupling constant for GdFeO_3 and YFeO_3 at room temperature in the approximation of the single-point charge lattice sum calculations.

9. The internal field as a function of temperature in the critical region in the range $0.60 < T/T_N < 0.99$ varies as the power 0.348 ± 0.005 of the temperature, i.e., approximately as the $\frac{1}{3}$ power and not as the $\frac{1}{2}$ power predicted by the molecular-field-theory approximation.

10. The isomer shift is independent of atomic number R at liquid-air temperature and is found to be about (0.61 ± 0.03) mm/sec using a source of Co^{57} in Cr, consistent with the idea that the main distortion occurs in the environment of the ion R^{3+} and not in the environment of Fe^{3+} , which remains octahedral.

11. The high-temperature specific heat of Fe for all the orthoferrites in the range of high temperature, as calculated from the temperature shift, is between (6.61 ± 0.63) cal/mole deg and (5.47 ± 0.63) cal/mole deg, in good agreement with the Dulong-Petit classical theory of the specific heat.

12. The Debye temperature of these compounds, as deduced from the temperature shift, is $(735 \pm 50)^\circ\text{K}$, in good agreement with that calculated from the Mössbauer fraction, $(800 \pm 50)^\circ\text{K}$.

13. The data for internal field, Curie temperature, isomer shift, quadrupole coupling, and all the lattice parameters for YFeO_3 fall between those for DyFeO_3 and HoFeO_3 . This is consistent with the fact that the ionic radius of Y falls between those of Dy and Ho.

ACKNOWLEDGMENTS

It is a pleasure to acknowledge the assistance of J. Lipkin and B. Sharon in the design and construction of much of the equipment used for the reported experiment. The authors are also indebted to Professor S. Alexander and Professor H. B. Callen for helpful discussions and comments.